

See discussions, stats, and author profiles for this publication at: <https://www.researchgate.net/publication/51598872>

# Mechanism of the Orotidine 5'-Monophosphate Decarboxylase-Catalyzed Reaction: Importance of Residues in the Orotate Binding Site

ARTICLE in BIOCHEMISTRY · SEPTEMBER 2011

Impact Factor: 3.02 · DOI: 10.1021/bi2012355 · Source: PubMed

---

CITATIONS

12

READS

26

## 6 AUTHORS, INCLUDING:



Bijoy Desai

University of Texas at Austin

8 PUBLICATIONS 77 CITATIONS

[SEE PROFILE](#)



Elena V Fedorov

Albert Einstein College of Medicine

62 PUBLICATIONS 2,147 CITATIONS

[SEE PROFILE](#)



Steven Almo

Albert Einstein College of Medicine

327 PUBLICATIONS 10,335 CITATIONS

[SEE PROFILE](#)



# NIH Public Access

## Author Manuscript

Biochemistry. Author manuscript; available in PMC 2012 October 4.

Published in final edited form as:  
*Biochemistry*. 2011 October 4; 50(39): 8497–8507. doi:10.1021/bi2012355.

## Mechanism of the Orotidine 5'-Monophosphate Decarboxylase-Catalyzed Reaction: Importance of Residues in the Orotate Binding Site<sup>†</sup>

Vanessa liams<sup>‡</sup>, Bijoy J. Desai<sup>‡</sup>, Alexander A. Fedorov<sup>§</sup>, Elena V. Fedorov<sup>§</sup>, Steven C. Almo<sup>§</sup>, and John A. Gerlt<sup>‡,\*</sup>

<sup>‡</sup>Departments of Biochemistry and Chemistry, University of Illinois at Urbana-Champaign, Urbana, IL

<sup>§</sup>Department of Biochemistry, Albert Einstein College of Medicine, Bronx, NY 10461

### Abstract

The reaction catalyzed by orotidine 5'-monophosphate decarboxylase (OMPDC) is accompanied by exceptional values for the rate enhancement [ $k_{\text{cat}}/k_{\text{non}} = 7.1 \times 10^{16}$ ] and catalytic proficiency [ $(k_{\text{cat}}/K_M)/k_{\text{non}} = 4.8 \times 10^{22} \text{ M}^{-1}$ ]. Although a stabilized vinyl carbanion/carbene intermediate is located on the reaction coordinate, the structural strategies by which the reduction in the activation energy barrier is realized remain incompletely understood. This laboratory recently reported that “substrate destabilization” by Asp 70 in the OMPDC from *Methanothermobacter thermoautotrophicus* (MtOMPDC) lowers the activation energy barrier by ~5 kcal/mol (contributing  $\sim 2.7 \times 10^3$  to the rate enhancement) [K. K. Chan, B. M. Wood, A. A. Fedorov, E. V. Fedorov, H. J. Imker, T. L. Amyes, J. P. Richard, S. C. Almo, and J. A. Gerlt (2009) *Biochemistry* 48, 5518–31]. We now report that substitutions of hydrophobic residues in a pocket proximal to the carboxylate group of the substrate (Ile 96, Leu 123, and Val 155) with neutral hydrophilic residues decrease the value of  $k_{\text{cat}}$  by as much as 400-fold but have minimal effect on the value of  $k_{\text{ex}}$  for exchange of H6 of the FUMP product analog with solvent deuterium; we hypothesize that this pocket destabilizes the substrate by preventing hydration of the substrate carboxylate group. We also report that substitutions for Ser 127 that is proximal to O4 of the orotate ring decrease the value of  $k_{\text{cat}}/K_M$ , with the S127P substitution that eliminates hydrogen-bonding interactions with O4 producing a  $2.5 \times 10^6$ -fold reduction in the value of  $k_{\text{cat}}/K_M$ ; this effect is consistent with delocalization of the negative charge of the carbanionic intermediate on O4 to produce an anionic carbene intermediate and thereby provide a structural strategy for stabilization of the intermediate.

<sup>†</sup>This research was supported by an NIH Chemistry Biology Interface Training Grant under Ruth L. Kirschstein National Research Service Award T32GM070241 (to V.I.) and NIH GM065155 (to J.A.G.). Molecular graphics images were produced using the UCSF Chimera package from the Resource for Biocomputing, Visualization, and Informatics at the University of California, San Francisco (supported by NIH P41 RR-01081). The X-ray coordinates and structure factors for the following structures have been deposited in the Protein Data Bank with the indicated accession codes: the S127G mutant of MtOMPDC in the presence of azaUMP (PDB accession code 3LLD), the S127A mutant of MtOMPDC in the presence of azaUMP (PDB accession code 3SY5), the S127A mutant of MtOMPDC in the presence of BMP (PDB accession code 3SIZ), the S127P mutant of MtOMPDC in the presence of azaUMP (PDB accession code 3LLF), the I96S mutant of MtOMPDC in the presence of azaUMP (PDB accession code 3PBU), the I96S mutant of MtOMPDC in the presence of BMP (PDB accession code 3NQC), the I96T mutant of MtOMPDC in the presence of azaUMP (PDB accession code 3RPV), the I96T mutant of MtOMPDC in the presence of BMP (PDB accession code 3NQD), the L123N mutant of MtOMPDC in the presence of azaUMP (PDB accession code 3PBW), the L123N mutant of MtOMPDC in the presence of BMP (PDB accession code 3NQE), the L123S mutant of MtOMPDC in the presence of azaUMP (PDB accession code 3PBY), the L123S mutant of MtOMPDC in the presence of BMP (PDB accession code 3NQF), the V155D mutant of MtOMPDC in the presence of BMP (PDB accession code 3NQG), the V155S mutant of MtOMPDC in the presence of azaUMP (PDB accession code 3PC0), and the 155SS mutant of MtOMPDC in the presence of BMP (PDB accession code 3NQM).

\*To whom correspondence should be addressed: J.A.G.: Institute for Genomic Biology, University of Illinois, 1206 West Gregory Drive, Urbana, IL 61801. Phone: (217) 244-7414. Fax: (217) 333-0508. j-gerlt@uiuc.edu.

These observations provide additional information on the identities of the active site residues that contribute to the rate enhancement and, therefore, insights into the structural strategies for catalysis.

The reaction catalyzed by orotidine 5'-monophosphate decarboxylase (OMPDC) continues to attract attention because the structural bases for its impressive rate enhancement [ $k_{\text{cat}}/k_{\text{non}} = 7.1 \times 10^{16}$ ] and catalytic proficiency [ $(k_{\text{cat}}/K_M)/k_{\text{non}} = 4.8 \times 10^{22} \text{ M}^{-1}$ ] (1) are not well understood. A “vinyl carbanion” intermediate is on the reaction coordinate (Scheme 1): 1) the reactions catalyzed by the OMPDCs from *Saccharomyces cerevisiae* (ScOMPDC) and *Methanothermobacter thermoautotrophicus* (MtOMPDC) proceed with a product isotope effect of 1.0 (measured when the reaction is conducted in a 1:1 mixture of H<sub>2</sub>O and D<sub>2</sub>O) (2). Both enzymes also catalyze the exchange of H<sub>6</sub> of the UMP product and the activated 5-fluoroUMP (FUMP) product analog with solvent hydrogen (3, 4), although at rates that are less than those observed for decarboxylation of either OMP or 5-fluoroOMP. However, the structural strategies by which the activation energy barrier ( $\Delta G^\ddagger$ ) for decarboxylation of OMP is reduced by 23 kcal/mol have not yet been completely described.

Although “ground state destabilization” of the substrate’s carboxylate group by its presumed proximity to Asp 70 in a conserved hydrogen-bonding network (residue numbering for MtOMPDC) was proposed when structures for four OMPDCs were reported in 2000 [MtOMPDC (5), ScOMPDC (6), and the OMPDCs from *Bacillus subtilis* (7) and *Escherichia coli* (8)], that proposal has been criticized (9–11). Recently, we provided experimental evidence in support of “substrate destabilization” in which destabilizing interactions develop as the reaction coordinate is traversed (the value of the K<sub>M</sub> for the OMP is less than the K<sub>i</sub> for the UMP product in which the carboxylate group is absent, thereby discounting “ground state destabilization”) (4). Substitution of Asp 70 with an isosteric uncharged residue (D70N) or a less sterically demanding, uncharged residue (D70G) reduces the value of k<sub>cat</sub> for decarboxylation by a factor of ~2,700 (D70G) without significantly affecting the value of k<sub>ex</sub> for exchange of H<sub>6</sub> of FUMP with solvent hydrogen.

Wolfenden estimated the value of the pK<sub>a</sub> of H<sub>6</sub> of the UMP product in aqueous solution (~32) by measuring the temperature dependence of the rate constant for nonenzymatic exchange in a model compound (12). Richard and Amyes used the value of k<sub>ex</sub> for the OMPDC-catalyzed exchange of H<sub>6</sub> to calculate an upper limit on the value of the pK<sub>a</sub> of H<sub>6</sub> of UMP in the active site (~22) (3). The difference (~10 pK<sub>a</sub> units) provides a lower limit on the stabilization of the intermediate by its interactions with the active site (≥14 kcal/mol).

On the basis of the structure of ScOMPDC complexed with 1-(5'-phospho-β-D-ribofuranosyl)barbiturate (BMP; alternatively, 6-hydroxyUMP), Wolfenden and Short and their coworkers proposed that Lys 93 (Lys 72 in MtOMPDC) is positioned to both provide electrostatic stabilization of the (localized) negative charge at C6 and then protonate the intermediate to form the UMP product (6). This proposal was reiterated by Cleland and coworkers, who concluded that “the mechanism of this enzyme is fairly well understood” (13).

However, in 1997, before the availability of a structure for any OMPDC, Houk and Lee proposed that the negative charge of the “vinyl carbanion” intermediate is not localized to C6 as implied in the proposed role of Lys 72 (MtOMPDC) as an electrostatic catalyst but can be resonance delocalized to O4 to generate a “carbene” at C6 (C6 is neutral with an electron pair in the sp<sup>2</sup> orbital) (14). Furthermore, protonation of O4 by an active site acid was predicted to provide substantial stabilization of the “carbene” intermediate. However, the structures for divergent OMPDCs reveal the absence of an acidic functional group proximal to O4; instead, based on the structures of liganded complexes with anionic

NIH-PA Author Manuscript NIH-PA Author Manuscript NIH-PA Author Manuscript

intermediate analogs (BMP and azaUMP), O4 of the OMP substrate is assumed to participate in hydrogen-bonding interactions with the backbone amide of Ser 127 as well as a structurally conserved water molecule. Delocalization of the negative charge on O4 as the anionic transition state/intermediate is formed should increase the strengths of these hydrogen bonds as the proton affinity of O4 increases (15–19). Houk and coworkers noted this environment could stabilize the charge-delocalized anionic intermediate (20). However, the importance of these hydrogen bonding interactions in the OMPDC-catalyzed reactions has not been investigated.

Also, Wolfenden and Lewis recently reported that the rate of decarboxylation of 1-methylorotate, a model of OMP, is increased in solvents less polar than water (21). At the extreme, the rate enhancement was reported to be 6,100-fold in tetrahydrofuran, dioxane, or acetone. The slower reaction in water is attributed to more effective solvation of the anionic carboxylate group in the reactant than in the anionic transition state/vinyl carbanion intermediate. These effects are similar to a rate enhancement of  $>10^4$  reported by Lienhard and coworkers for the decarboxylation of 2-(1-carboxy-1-hydroxyethyl)thiamin pyrophosphate to yield 2-(1-hydroxyethyl)thiamin pyrophosphate performed in dimethylsulfoxide instead of water (22, 23). Again, these effects were attributed to diminished solvation of the reactant in the nonpolar solvents relative to the solvation of the transition state.

Although not noted by Wolfenden and Lewis, the active sites of all OMPDCs contain a hydrophobic cavity proximal to the presumed location for the carboxylate group of the bound OMP substrate. A reasonable hypothesis is that this hydrophobic cavity prevents solvation of the carboxylate group; because the negative charge of the anionic intermediate is delocalized to O4, the hydrophobic cavity is not expected to influence solvation of the transition state/intermediate. However, the importance of this hydrophobic cluster has not been previously noted, so its potential importance in “substrate destabilization” has not been tested.

In this manuscript we report the effects of site-directed substitutions for residues in the MtOMPDC that form the hydrophobic pocket proximal to the C6 carboxylate group as well as Ser 127 that hydrogen bonds to O4 of the substrate/vinyl carbanion intermediate *via* its backbone amide. Our results provide evidence that contradict the proposal that “the mechanism of this enzyme is fairly well understood” (13).

## MATERIALS AND METHODS

### Materials

azaUMP was purchased from R.I. Chemicals Inc. Barbiturate was purchased from Sigma. All solutions were prepared with Millipore Ultrapure filtered water. OMP, FOMP, FUMP, and BMP were prepared by published procedures (4, 13, 24, 25).

### Cloning, Site-Directed Mutagenesis, and Protein Expression and Purification

The gene encoding MtOMPDC was previously cloned from *Methanothermobacter thermoautotrophicus* strain *Delta H* genomic DNA into pET-15b vector (Novagen) (4, 24). This plasmid served as the template for site-directed mutagenesis by the overlap extension procedure. Primers with the desired mutations (Eurofins MWG Operon) were combined with external primers to generate two gene fragments. The PCR product was digested by *Nde* I and *Bam* HI (Promega) followed by ligation into pET-15b. DNA sequencing at the University of Illinois Core Sequencing Facility confirmed the desired sequences. The mutants were purified from a kanamycin-resistant *pyrF*<sup>-</sup> strain of *E. coli* generated using Wanner’s method for chromosomal disruptions (26); a chloramphenicol-resistant auxiliary

plasmid, pTara, a gift from Professor John Cronan at the University of Illinois, supplied the T7 RNA polymerase for transcription from pET-15b. The mutant proteins were isolated by published procedures (4, 24).

### Enzymatic Assays

All assays were performed at 25°C and in 10 mM MOPS, pH 7.1, containing 100 mM NaCl following published procedures (4, 24). Because the values of  $K_M$  for wild type and most mutants are < 5  $\mu$ M, they cannot be quantitated by measuring the initial velocity as a function of initial substrate concentration. Instead, as described elsewhere (24), the values of  $k_{cat}/K_M$  were determined from the first-order decay of the absorbance when the concentration of remaining substrate was  $\leq$  20% of the estimated  $K_M$  value; the values of  $k_{cat}$  were determined in separate assays with substrate concentrations exceeding the estimated values of  $K_M$  by a factor  $\geq$  10. The kinetic constants for mutants with values of  $K_M$  values > 20  $\mu$ M were measured by initial velocity measurements.

### Exchange of H6 of FUMP

Exchange of the H6 proton of FUMP (5 mM) was measured in 100 mM glycylglycine (pD 9.35, I = 0.1 M with NaCl) using  $^1$ H and  $^{19}$ F NMR spectroscopies as described elsewhere (3, 4).

### Crystallization and Data Collection

Eight different crystal forms (Table 1) of mutants of MtOMPDC liganded with azaUMP were grown by the hanging drop method at room temperature: 1) S127G•azaUMP, 2) S127A•azaUMP, 3) S127P•azaUMP, 4) I96S•azaUMP, 5) I96T•azaUMP, 6) L123N•azaUMP, 7) L123S•azaUMP, and 8) V155S•azaUMP. The protein solutions contained the mutant protein (30 mg/mL) in 20 mM Hepes, pH 7.5, 150 mM NaCl, 3 mM DTT, and 40 mM azaUMP. The precipitants were the following:

1. For S127G•azaUMP, the precipitant contained 20% PEG 3350 and 0.15 M DL-malate, pH 7.0.
2. For S127A•azaUMP, the precipitant contained 30% PEG 400, 0.1 M Hepes (pH 7.5), and 0.2 M sodium chloride.
3. For S127P•azaUMP, the precipitant contained 60% tacsimate, pH 7.0.
4. For I96S•azaUMP, the precipitant contained 30% PEG 4000, 0.1 M sodium citrate, pH 5.6, and 0.2 M ammonium acetate.
5. For I96T•azaUMP, the precipitant contained 30% PEG 4000, 0.1 M sodium citrate, pH 5.6, and 0.2 M ammonium acetate.
6. For L123N•azaUMP, the precipitant contained 25% PEG 3350, 0.1 M Bis-Tris, pH 5.5, and 0.2 M lithium sulfate.
7. For L123S•azaUMP, the precipitant contained 20% PEG 8000, 0.1 M sodium cacodylate, pH 6.5, and 0.2 M magnesium acetate.
8. For V155S•azaUMP, the precipitant contained 30% PEG ME 5000, 0.1 M MES, pH 6.5, and 0.2 M ammonium sulfate.

Seven different crystal forms (Table 2) of mutants of MtOMPDC liganded with BMP were grown by the hanging drop method at room temperature: 1) S127A•BMP, 2) I96S•BMP, 3) I96T•BMP, 4) L123N•BMP, 5) L123S•BMP, 6) V155D•BMP, and 7) V155S•BMP. The protein solutions contained the mutant protein (30 mg/mL) in 20 mM Hepes, pH 7.5, 150 mM NaCl, 3mM DTT, and 40mM BMP. The precipitants were the following:

1. For S127A•BMP, the precipitant contained 30% PEG 4000, 0.1 M sodium citrate (pH 5.6), and 0.2 M ammonium acetate.
2. For I96S•BMP, the precipitant contained 60% tacsimate, pH 7.0.
3. For I96T•BMP, the precipitant contained 25% PEG 3350, 0.1 M Bis-Tris, pH 6.5, and 0.2 M MgCl<sub>2</sub>.
4. For L123N•BMP, the precipitant contained 30% PEG ME 2000, and 0.1 M potassium thiocyanate.
5. For L123S•BMP, the precipitant contained 25% PEG 3350, 0.1M Bis-Tris, pH 6.5, and 0.2 M MgCl<sub>2</sub>.
6. For V155D•BMP, the precipitant contained 1.4M sodium citrate, and 0.1 M Hepes, pH 7.5.
7. For V155S•BMP, the precipitant contained 2.4 M sodium malonate, pH 7.0.

Prior to data collection, the crystals were transferred to cryoprotectant solutions composed of their mother liquor and 20% glycerol and flash-cooled in a nitrogen stream. All X-ray diffraction data sets (Tables 1 and 2) were collected at the NSLS X4A beamline (Brookhaven National Laboratory) on an ADSC CCD detector. Diffraction intensities were integrated and scaled with programs DENZO and SCALEPACK (27). The data collection statistics are given in Tables 1 and 2.

### Structure Determination and Model Refinement

All 15 structures (Tables 1 and 2) were solved by molecular replacement with the fully automated molecular replacement pipeline BALBES (28), using only input diffraction and sequence data. Partially refined structures of all 15 crystal forms (Tables 1, 2) were the outputs from BALBES without any manual intervention. Subsequent several iterative cycles of refinement were performed for each crystal form including model rebuilding with COOT (29), refinement with PHENIX (30), and automatic model rebuilding with ARP (31).

In each structure, the polypeptides are arranged as dimers with the monomers connected by a noncrystallographic two-fold axis. The active site loops, chain segment 181–189, are well-defined in each structure. Each structure also has well-ordered density for the inhibitor in each active site. No residues (other than Gly) lie in disallowed regions of the Ramachandran plots in the various structures.

Representative electron density for the S127P mutant liganded with azaUMP is shown in Figure 1.

Final crystallographic refinement statistics for all determined OMPDC structures are provided in the Tables 1 and 2.

## RESULTS AND DISCUSSION

As summarized in the Introduction, the value of  $\Delta G^\ddagger$  for decarboxylation of OMP is reduced by 23 kcal/mol in the active sites of homologous, but divergent, OMPDCs, although the structural strategies that accomplish this reduction remain uncertain. In this manuscript we describe studies of two features of the active site of MtOMPDC that have not been previously investigated: 1) a hydrophobic pocket proximal to C6, and 2) Ser 127 that interacts with N3 and O4 of the orotate moiety. On the basis of the experiments described in this manuscript, we conclude that both features contribute to the reduction in  $\Delta G^\ddagger$ .

## Importance of the Hydrophobic Pocket

We previously reported structures of wild type MtOMPDC liganded with BMP and azaUMP, analogs of the transition state/carbonium intermediate, as well as with 5,6-dihydroOMP ( $H_2\text{OMP}$ ), a stable analog of OMP that may be a mimic of “substrate destabilization” (4, 32). The structures of the orotate binding pockets are superimposable, although the active site of the complex with BMP contains an “extra” water molecule hydrogen-bonded to O6 of the 6-OH uracil (barbiturate) ring.

The active site of the previously reported complex of wild type MtOMPDC with  $H_2\text{OMP}$  is shown in Figure 2. The C6-carboxylate group “points” into the hydrophobic cavity that is formed by the side chains of Ile 96, Leu 123, Val 155, and Pro 180. No water molecules are observed in the hydrophobic cavity. Although these could be brought into the active site by hydrogen bonding interactions with the carboxylate group, the hydrophobic side cavity would prevent completion of their preferred tetrahedral hydrogen bonding interactions, thereby making their presence in the active site unfavorable.

We constructed polar substitutions for Ile 96, Leu 123, and Val 155, i.e., I96S, I96T, L123N, L123S, V155D, and V155S, to increase the polarity of the active site cavity; these “targets” for study were based on the report from Wolfenden and Lewis that the nonenzymatic decarboxylation of OMP analogs is increased as the solvent polarity is decreased because the negative charge of the departing carboxylate group is not stabilized (21). Therefore, we hypothesized that introduction of polar residues in this cavity (and possible “new” water molecules that can interact with hydrogen bond donors/acceptors) would decrease the value of  $k_{\text{cat}}$ . We did not construct substitutions for Pro 180 because it is located at the N-terminus of the active site loop: we recently reported that the interaction of the sequence-proximal Val 182 in the loop with the  $(\beta/\alpha)_8$ -barrel scaffold favors formation of the closed, active conformation of the enzyme (32); therefore, we were concerned that polar substitutions for Pro 180 could influence the kinetic constants by perturbing the distribution between the open and closed conformations of the enzyme.

## Structures of the Mutants with Polar Substitutions for Hydrophobic Pocket Residues

We determined structures for all six hydrophobic pocket mutants in the presence of BMP (Figure 3 and 4); we also determined structures for five of the mutants (except V155D) in the presence of azaUMP (Figures 5 and 6). In all of the structures, the side chains of the active site residues, including Asp 70, Lys 72, and Asp 75 (from the adjacent polypeptide in the dimer) superimpose well with those of the BMP/azaUMP-ligated structures of wild type MtOMPDC (Figures 3 and 5), providing evidence that the interactions of the transition state/vinyl carbonion intermediate with the active site are preserved in each mutant.

Therefore, in our interpretation of their kinetic constants, we assume that changes in  $k_{\text{cat}}$  arise from the altered environment provided by the now polar cavity adjacent to the carboxylate group of OMP.

In five of the six BMP-ligated mutant structures (I96S, I96T, L123N, L123S, and V155S), two “conserved” water molecules which hydrogen bond to O4 and O6 of BMP undergo small changes in position (Figures 3 and 4). The water proximal to O4 is conserved in all structurally characterized OMPDCs and may participate in stabilization of the negative charge that is localized on O4 of the vinyl carbonion/carbene intermediate; the water proximal to O6 of BMP likely is not present when the OMP substrate binds (recall that the complex of wild type MtOMPDC with  $H_2\text{OMP}$  does not contain any water molecules). The active site of the BMP-ligated L123S contains a third (“new”) water that is stabilized by its proximity to the waters adjacent to O4 and O6, the O6 oxyanion of BMP, and the hydroxyl group of the L123S side chain.

Wild type MtOMPDC binds azaUMP in the *syn*-conformation, in which O2 is hydrogen bonded to the carboxamide NH<sub>2</sub> group of Gln 185 and N3 is hydrogen bonded to the OH group of Ser 127. However, in the mutants, azaUMP is bound in the *anti*-conformation in which the pyrimidine ring is rotated by 180° around the glycosidic bond (Figure 6). With this geometry and in each structure, O2 is hydrogen bonded to a “new” water molecule that is not observed in the wild type azaUMP complex (analogous to the “conserved” water molecules proximal to O6 in the BMP-ligated structures). The substitutions for Val 155 and Ile 96 perturb the position of the Leu 123 side chain, thereby altering the shape of the pocket. Also, in the L123N and V155S mutants, a second “new” water is hydrogen bonded to N3 of the 6-azauracil moiety.

### Kinetic Constants for the Mutants with Polar Substitutions for Hydrophobic Pocket Residues

For wild type MtOMPDC, decarboxylation of OMP is fully rate-determining for  $k_{\text{cat}}$ , although  $k_{\text{cat}}/K_M$  has a small inverse dependence on viscosity, indicating that both chemical and physical steps determine its value (24). Therefore, changes in  $k_{\text{cat}}$  report on changes in  $\Delta G^\ddagger$  for decarboxylation. We also previously demonstrated that substitutions for Asp 70 decrease the value of  $k_{\text{cat}}$  but do not alter the value of  $k_{\text{ex}}$ , (exchange of H6 of the UMP product or the FUMP product analog with solvent), thereby providing support for the occurrence of the vinyl carbanion intermediate (obtained either from decarboxylation of OMP or exchange of H6 of the UMP product) on the reaction coordinate (4). We interpreted the effects of the substitutions for Asp 70 as evidence for “substrate destabilization” during the transition from the open, inactive conformation to the closed, active conformation, presumably by unfavorable electrostatic (and steric) interactions with the substrate carboxylate group.

We measured the effects of the various polar substitutions for the hydrophobic pocket residues on the values of 1)  $k_{\text{cat}}$  and  $K_M$  for decarboxylation of OMP, and 2)  $k_{\text{ex}}$  for exchange of H6 of the more reactive product analog 5-fluoroUMP; these are presented in Table 3.

The values of  $k_{\text{cat}}$  are decreased from 6- to 400-fold for the various neutral polar substitutions; for the V155D substitution the value of  $k_{\text{cat}}$  is decreased by ~10,000-fold. However, the values of  $K_M$  for the mutants are increased < 3-fold, including for the V155D mutant. Thus, each of the polar substitutions decreases the rate at which the vinyl carbanion intermediate is formed by decarboxylation but do not alter the conformational equilibrium between the open, inactive and closed, active conformations (32).

However, for Ile 96 and Val 155 (including V155D for which the value of  $k_{\text{cat}}$  is substantially decreased), the values of  $k_{\text{ex}}$  are not significantly altered by the substitutions. The simplest interpretation is that the stability of the anionic intermediate is not affected by the substitutions. That these substitutions increase  $\Delta G^\ddagger$  for decarboxylation but not exchange suggests that the hydrophobic pocket contributes to the reduction in  $\Delta G^\ddagger$  by placing the substrate carboxylate in a destabilizing, hydrophobic environment (“hydrophobic stress”).

For L123N and L123S the values of  $k_{\text{ex}}$  are decreased more than the values of  $k_{\text{cat}}$ . A possible explanation is provided by the structures of azaUMP complexes of these mutants in which an “extra” water is located proximal to the pyrimidine moiety in each active site, providing the potential to influence either the rate of formation of the anion intermediate by proton abstraction or the stability of the intermediate.

Thus, for the neutral polar substitutions, the decreases in  $k_{\text{cat}}$  support the hypothesis that enhanced polarity proximal to C6 of the orotate substrate decreases the rate of decarboxylation by stabilizing the anionic carboxylate group relative to the anionic intermediate, as suggested by Wolfenden and Lewis to explain the enhanced rate of decarboxylation in solvents less polar than water. The very substantial effect of the V155D substitution likely can be best explained by unfavorable electrostatic interactions with the substrate carboxylate group as the reaction coordinate for decarboxylation is traversed.

We note that a hydrophobic pocket proximal to the substrate carboxylate group is conserved in all OMPDCs, despite considerable divergence in sequence, so all OMPDCs presumably adopt this structural strategy for reducing the value of  $\Delta G^\ddagger$ .

### Independent Mechanisms for “Ground State Destabilization”?

As summarized in the Introduction, we recently reported that the D70N and D70G substitutions also decrease the value of  $k_{\text{cat}}$  without influencing the value of  $k_{\text{ex}}$ ; these effects were interpreted as evidence for “ground state destabilization” of the substrate’s carboxylate by its proximity to the anionic carboxylate group of Asp 70 (4). We now have concluded that the hydrophobic pocket prevents stabilization of the substrate carboxylate group relative to the transition state/vinyl carbanion intermediate. Therefore, we constructed the D70N/I96S, D70N/L123S, and D70N/V155S double mutants in an attempt to obtain evidence that these structurally distinct effects are independent contributors to the reduction in  $\Delta G^\ddagger$ .

The values of  $k_{\text{cat}}$ ,  $K_M$ , and  $k_{\text{ex}}$  for the double mutants also are reported in Table 3. The values of  $k_{\text{cat}}$  for the single D70N, V155S and I96S mutants are reduced by factors between 200- and 400-fold. For the double mutants with these residues, the values of  $k_{\text{cat}}$  are reduced by factors that approximate the reductions observed for the single mutants, i.e., the increases in  $\Delta G^\ddagger$  are additive, supporting the conclusion that electrostatic repulsion by Asp 70 and “hydrophobic stress” by the hydrophobic pocket independently contribute to “substrate destabilization” as the transition state for decarboxylation is achieved (we could not measure the values of  $K_M$  by analysis of the first order decay in absorbance at low substrate concentrations because of the very slow rates of reaction).

The values for  $k_{\text{ex}}$  for the D70N/I96S and D70N/V155S double mutants are each less than that for the D70N mutant (by a factor of ~8) but are significant greater than those expected if the effects of the individual mutants were additive (by 22- and 44-fold, respectively). Although not “perfect”, these data support the suggestion that the increases in  $\Delta G^\ddagger$  for exchange of H6 are not additive, i.e., the effects of the hydrophobic pocket and D70N are independent contributors to “substrate destabilization” with neither contributing significantly to intermediate/transition state destabilization.

Like the L123S single mutant, the D70N/L123S double mutant shows “anomalous” behavior: the value of  $k_{\text{cat}}$  is 10-fold lower than the value predicted if the effects on  $\Delta G^\ddagger$  were additive; however, the value of  $k_{\text{ex}}$  is reduced 1500-fold from that observed for wild type MtOMPDC and 300-fold from those observed for D70N/I96S and D70N/V155S double mutants. Again, these lower than expected values for  $k_{\text{cat}}$  and  $k_{\text{ex}}$  may result from the “extra” water molecule proximal to the pyrimidine moiety.

Thus, we conclude that the reduction in  $\Delta G^\ddagger$  by MtOMPDC involves at least two structurally independent mechanisms to achieve “substrate destabilization”.

## Importance of Ser 127 in Stabilization of an Anionic Transition State/Intermediate

As proposed by Houk and coworkers (14, 20), a hydrogen bond donor adjacent to O4 of the OMP substrate could contribute significantly to the reduction in  $\Delta G^\ddagger$  by stabilization of the transition state/anionic intermediate as developing negative charge in the pyrimidine moiety is delocalized to O4. Structural studies of divergent OMPDCs reveal that O4 of the substrate always is hydrogen bonded to the backbone NH group of a conserved Ser (or, occasionally, Thr) in the loop following the fifth  $\beta$ -strand of the ( $\beta/\alpha$ )<sub>8</sub>-barrel domain (Ser 127 in MtOMPDC) as well as the spatially conserved water molecule. In addition, the side chain OH group of the Ser residue is hydrogen bonded to the proton on N3. The quantitative importance of these interactions in the reduction of  $\Delta G^\ddagger$  has not been reported.

We constructed and kinetically characterized the S127A, S127G, and S127P mutants of MtOMPDC to obtain information about the importance of these interactions; we also obtained structures of the S127A, S127G, and S127P mutants liganded with azaUMP. The S127A and S127G substitutions allow the importance of the interactions between the side chain OH group and N3 of the orotate moiety to be investigated. The S127P substitution replaces the backbone NH group with Cy of the side chain; although we recognized that this likely would introduce a steric clash with O4 of the OMP substrate, we considered this mutant to be worthwhile to characterize.

## Structures of the S127A, S127G, and S127P Mutants

We determined structures for the Ala, Gly, and Pro substitutions for Ser 127 in the presence of azaUMP. The structures of the active sites of the mutants superimpose well with that of wild type MtOMPDC complexed with azaUMP (Figure 7), with small deviations in backbone geometry observed for residue 127 and the two flanking residues (Met 126 and His 128). In the structure of the S127G mutant, a water molecule occupies the position of the OH group of the Ser residue in wild type MtOMPDC and is hydrogen bonded to both N3 of the pyrimidine ring and the carboxamide group of Gln 185; this water molecule is not present in the S127A, presumably because of steric exclusion. The positions of the side chains of the active site residues, including Asp 70, Lys 72, and Asp 75 (from the adjacent polypeptide), are not affected by the substitutions for Ser 127.

The positions of the ligands in the various azaUMP-ligated complexes are shifted from the position in wild type MtOMPDC, with the effects most pronounced for the 6-azauracil moiety (Figures 6 and 7). For example, in the S127P mutant, O4 is displaced by 1.1 Å from the positions of O4 in the wild type and by 1.5 Å from the positions of O4 in the S127A and S127G mutants because of the steric clash with the aliphatic Pro ring; also, N6 is positioned 0.6 Å closer to the carboxylate group of Asp 70 and 0.3 Å closer to the  $\epsilon$ -ammonium group of Lys 72 than the wild type. Although these changes complicate precise structure-based interpretation of the kinetic constants (*vide infra*), we decided that characterization of this substitution would provide relevant information about the role of Ser 127.

## Kinetic Constants for the S127A, S127G, and S127P Mutants

The S127A and S127G substitutions retain the interaction between O4 of the pyrimidine ring and the backbone NH of residue 127, although these alter the interactions between the side chain and N3 of the pyrimidine ring as well as the carboxamide group of Gln 185.

For both mutants, the values of  $K_M$  are increased (Table 4), consistent with the proposal that the hydrogen bond between the OH group of Ser 127 and the carboxamide group of Gln 185 provides a “clamp” for stabilizing the closed, active conformation of the enzyme (33). The value of  $k_{cat}$  is reduced ~130-fold for the S127A mutant and ~18-fold for the S127G mutant. The reduction for the Ala substitution suggests that a hydrogen bond between the OH group

of Ser 127 and the proton of N3 provides stabilization of the enhanced, delocalized anionic charge in the pyrimidine ring that occurs as the vinyl anion/carbene intermediate is formed. The partial “rescue” observed for the Gly substitution is explained by the presence of a water molecule that occupies the position of the Ser OH group, thereby mimicking the OH group.

The values of  $k_{cat}$  and  $K_M$  cannot be measured for the S127P mutant; the value of  $k_{cat}/K_M$  is determined from the linear dependence of velocity on substrate concentration. The value so determined is reduced by an impressive factor of  $2.5 \times 10^6$ . Quantitative interpretation of this effect in the context of the interaction between O4 and the backbone NH group of Ser 127 is equivocal. The structure reveals, as expected, that the Pro substitution alters the position of the pyrimidine ring in the active site: O4 of the ligand is displaced 1.1 Å from the position of O4 in the wild type and 1.5 Å from those in the S127A and S127G mutants; it obviously cannot form a hydrogen bond with the backbone. However, the position of N6 (homologue of C6 in the vinyl anion/carbene) relative to Ne of Lys 72 is decreased by 0.3 Å in the mutant relative to wild type (2.7 Å vs. 3.0 Å, respectively). If electrostatic effects between Lys 72 and the anionic intermediate are of primary importance in reducing the value of  $\Delta G^\ddagger$ , the decrease in the distance in the S127P mutant would be expected to have only a “minor” effect on  $k_{cat}$  (23% assuming Coulomb’s law applies to the interaction between the ε-ammonium group of Lys 72 and the anionic C6, i.e., no charge delocalization to form a carbene in the anionic intermediate). Thus, the very large reduction in the value of  $k_{cat}$  observed for the S127P mutant is an indication that the interaction of O4 with the backbone NH of Ser 127 contributes significantly to stabilization of the vinyl anion/carbene intermediate.

Houk and Lee proposed an anionic carbene resonance structure for the anionic intermediate in which negative charge is delocalized to O4 (14, 20). Making the reasonable assumption that the strength of the hydrogen bond to the backbone NH of Ser 127 increases as negative charge is delocalized to O4, this interaction could provide significant stabilization of the intermediate and contribute to the reduction in  $\Delta G^\ddagger$  (17). However, quantitation of this stabilization is difficult because 1) removal of the O4 hydrogen bond acceptor, i.e., 4-deoxyuracil, will also result in loss of a proton from N3, thereby eliminating the hydrogen bond to Oβ of Ser 127, and 2) alteration of the hydrogen bond donor (the NH of Ser 127) cannot be readily accomplished, even with unnatural mutagenesis (in principle, replacement of the peptide bond linkage with an ester linkage may be possible, but, in practice, ribosome-mediated synthesis of depsipeptide linkages in protein is difficult).

## Conclusions

The structural strategies by which the remarkable rate enhancement achieved by OMPDCs [ $k_{cat}/k_{non} = 7.1 \times 10^{16}$ ] are not well-defined. Although electrostatic stabilization of the anionic intermediate by Lys 72 is frequently used to explain the rate acceleration, we are investigating the role of other active site residues. We previously demonstrated that Asp 70 contributes modestly to the rate enhancement by destabilization of the substrate. We now conclude that a hydrophobic cavity proximal to the carboxylate group of the substrate also destabilizes the substrate, presumably by preventing the carboxylate group from being stabilized by waters of hydration when it is bound in the active site. This effect is also modest, but likely is employed by all OMPDCs given that residues in the hydrophobic cavity are conserved. The importance of hydrogen bonding interactions with O4 of the pyrimidine moiety of the substrate is more difficult to investigate experimentally because the hydrogen bond donor is a peptide backbone NH group of Ser 127. Replacement of Ser 127 with proline (S127P) has a large effect on  $k_{cat}/K_M$  (a reduction of  $2.5 \times 10^6$ ), supporting the proposal by Lee and Houk that the hydrogen bond between O4 of the substrate and the backbone NH is important in reducing  $\Delta G^\ddagger$ .

## Abbreviations

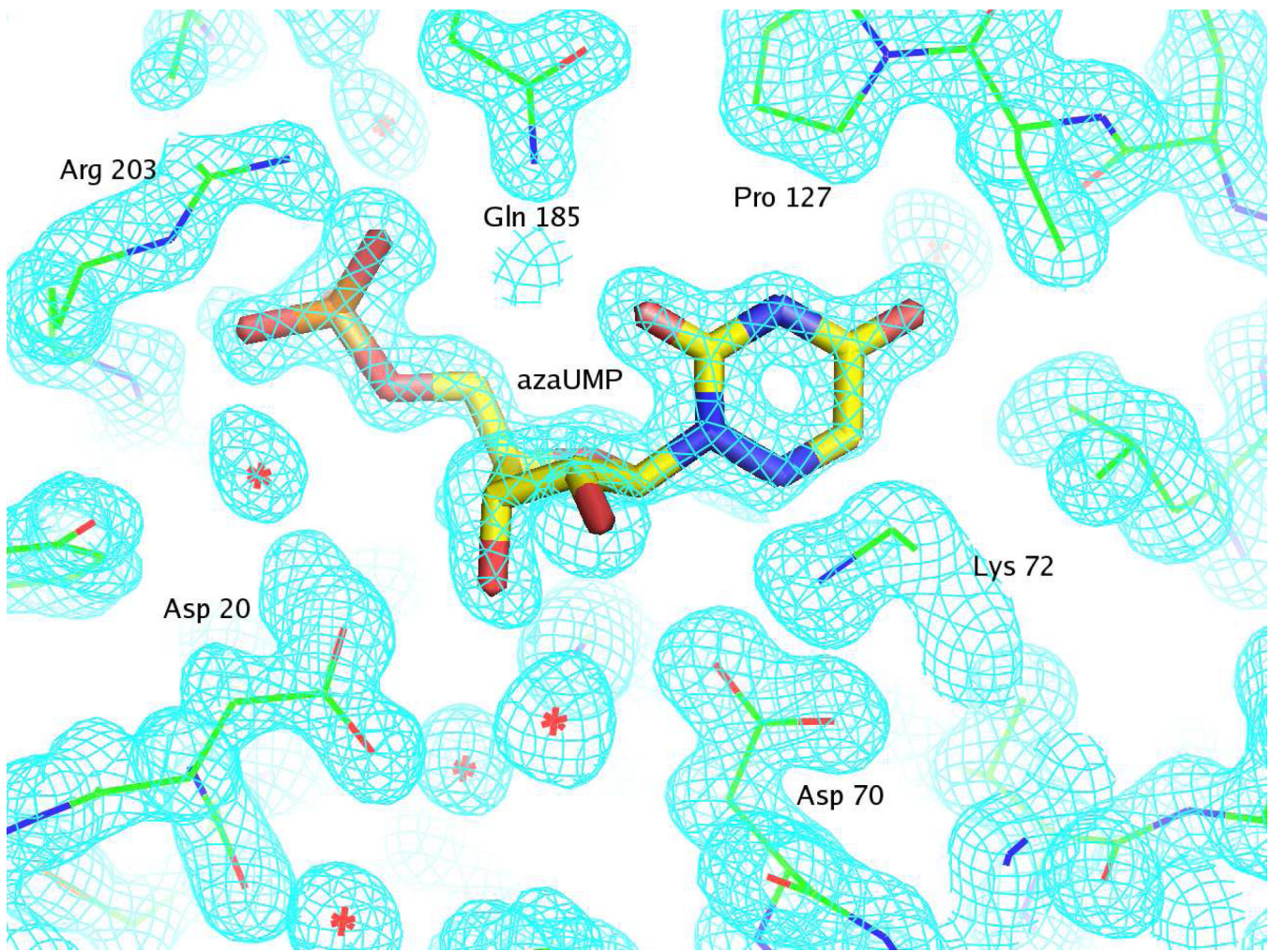
<b>FOMP</b>	5-fluoroorotidine 5'-monophosphate
<b>FUMP</b>	5-fluoroUMP
<b>azaUMP</b>	6-azauridine 5'-monophosphate
<b>BMP</b>	1-(5'-phospho-β-D-ribofuranosyl)barbituric acid
<b>MtOMPDC</b>	OMPDC from <i>Methanothermobacter thermoautotrophicus</i>
<b>OMP</b>	orotidine 5'-monophosphate
<b>OMPDC</b>	orotidine 5'-monophosphate decarboxylase
<b>ScOMPDC</b>	OMPDC from <i>Saccharomyces cerevisiae</i>
<b>WT</b>	wild type

## REFERENCES

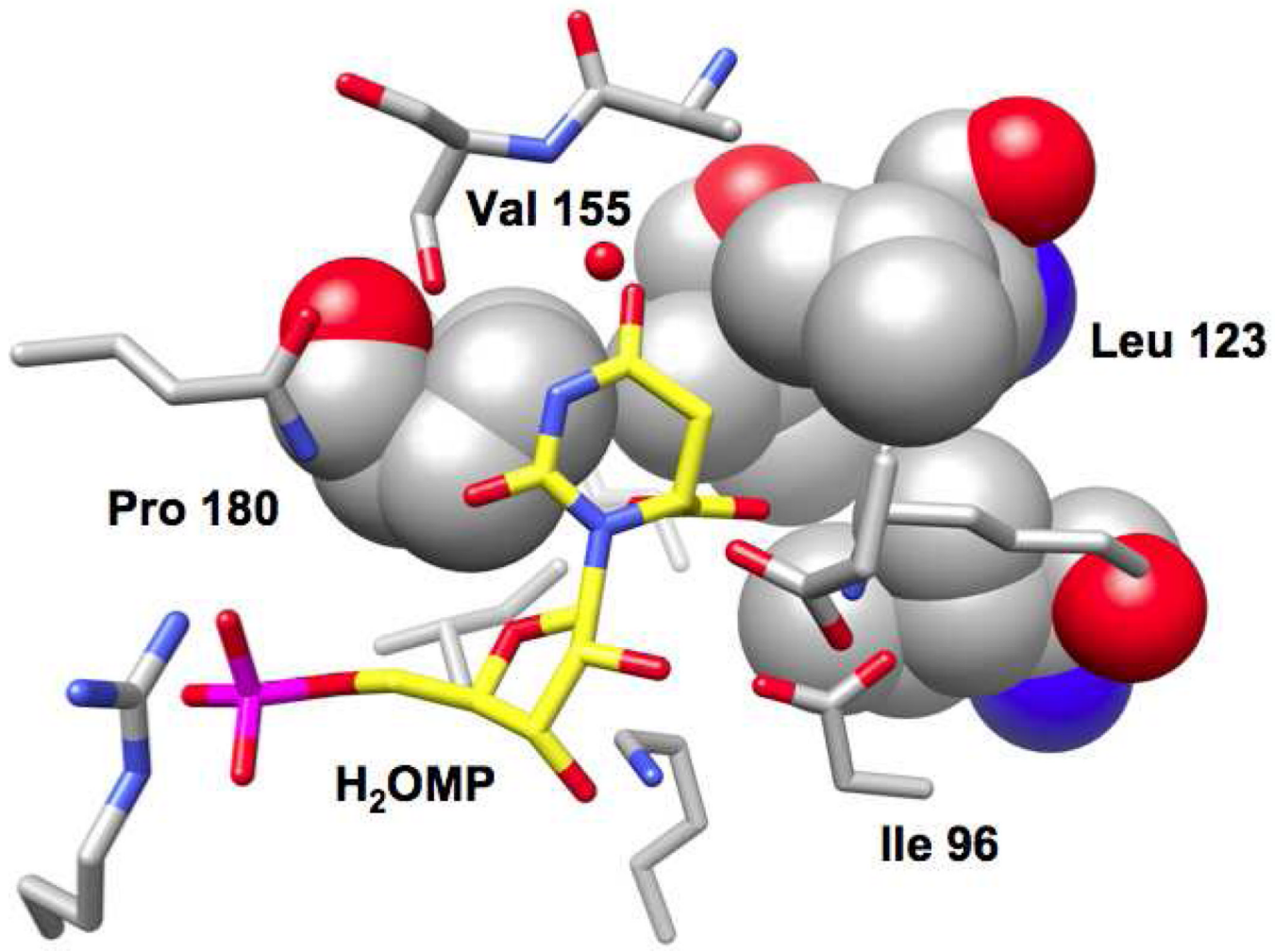
1. Radzicka A, Wolfenden R. A proficient enzyme. *Science*. 1995; 267:90–93. [PubMed: 7809611]
2. Toth K, Amyes TL, Wood BM, Chan K, Gerlt JA, Richard JP. Product deuterium isotope effect for orotidine 5'-monophosphate decarboxylase: evidence for the existence of a short-lived carbanion intermediate. *J Am Chem Soc*. 2007; 129:12946–12947. [PubMed: 17918849]
3. Amyes TL, Wood BM, Chan K, Gerlt JA, Richard JP. Formation and stability of a vinyl carbanion at the active site of orotidine 5'-monophosphate decarboxylase: pKa of the C-6 proton of enzyme-bound UMP. *J Am Chem Soc*. 2008; 130:1574–1575. [PubMed: 18186641]
4. Chan KK, Wood BM, Fedorov AA, Fedorov EV, Imker HJ, Amyes TL, Richard JP, Almo SC, Gerlt JA. Mechanism of the orotidine 5'-monophosphate decarboxylase-catalyzed reaction: evidence for substrate destabilization. *Biochemistry*. 2009; 48:5518–5531. [PubMed: 19435314]
5. Wu N, Mo Y, Gao J, Pai EF. Electrostatic stress in catalysis: structure and mechanism of the enzyme orotidine monophosphate decarboxylase. *Proc Natl Acad Sci U S A*. 2000; 97:2017–2022. [PubMed: 10681441]
6. Miller BG, Hassell AM, Wolfenden R, Milburn MV, Short SA. Anatomy of a proficient enzyme: the structure of orotidine 5'-monophosphate decarboxylase in the presence and absence of a potential transition state analog. *Proc Natl Acad Sci U S A*. 2000; 97:2011–2016. [PubMed: 10681417]
7. Appleby TC, Kinsland C, Begley TP, Ealick SE. The crystal structure and mechanism of orotidine 5'-monophosphate decarboxylase. *Proc Natl Acad Sci U S A*. 2000; 97:2005–2010. [PubMed: 10681442]
8. Harris P, Navarro Poulsen JC, Jensen KF, Larsen S. Structural basis for the catalytic mechanism of a proficient enzyme: orotidine 5'-monophosphate decarboxylase. *Biochemistry*. 2000; 39:4217–4224. [PubMed: 10757968]
9. Warshel A, Strajbl M, Villa J, Florian J. Remarkable rate enhancement of orotidine 5'-monophosphate decarboxylase is due to transition-state stabilization rather than to ground-state destabilization. *Biochemistry*. 2000; 39:14728–14738. [PubMed: 11101287]
10. Warshel A, Florian J, Strajbl M, Villa J. Circe effect versus enzyme preorganization: what can be learned from the structure of the most proficient enzyme? *Chembiochem*. 2001; 2:109–111. [PubMed: 11828433]
11. Kamerlin SC, Chu ZT, Warshel A. On catalytic preorganization in oxyanion holes: highlighting the problems with the gas-phase modeling of oxyanion holes and illustrating the need for complete enzyme models. *J Org Chem*. 2010; 75:6391–6401. [PubMed: 20825150]
12. Sievers A, Wolfenden R. Equilibrium of formation of the 6-carbanion of UMP, a potential intermediate in the action of OMP decarboxylase. *J Am Chem Soc*. 2002; 124:13986–13987. [PubMed: 12440884]

13. Van Vleet JL, Reinhardt LA, Miller BG, Sievers A, Cleland WW. Carbon isotope effect study on orotidine 5'-monophosphate decarboxylase: support for an anionic intermediate. *Biochemistry*. 2008; 47:798–803. [PubMed: 18081312]
14. Lee JK, Houk KN. A proficient enzyme revisited: the predicted mechanism for orotidine monophosphate decarboxylase. *Science*. 1997; 276:942–945. [PubMed: 9139656]
15. Gerlt JA, Gassman PG. An Explanation for Rapid Enzyme-Catalyzed Proton Abstraction from Carbon Acids: The Importance of Late Transition States in Concerted Mechanisms. *J. Am. Chem. Soc.* 1993; 115:11552–11569.
16. Cleland WW, Kreevoy MM. Low-barrier hydrogen bonds and enzymic catalysis. *Science*. 1994; 264:1887–1890. [see comments]. [PubMed: 8009219]
17. Shan SO, Herschlag D. The change in hydrogen bond strength accompanying charge rearrangement: implications for enzymatic catalysis. *Proc Natl Acad Sci U S A*. 1996; 93:14474–14479. [PubMed: 8962076]
18. Gerlt JA, Kreevoy MM, Cleland W, Frey PA. Understanding enzymic catalysis: the importance of short, strong hydrogen bonds. *Chem Biol*. 1997; 4:259–267. [PubMed: 9195866]
19. Cleland WW, Frey PA, Gerlt JA. The low barrier hydrogen bond in enzymatic catalysis. *J Biol Chem*. 1998; 273:25529–25532. [PubMed: 9748211]
20. Houk KN, Lee JK, Tantillo DJ, Bahmanyar S, Hietbrink BN. Crystal structures of orotidine monophosphate decarboxylase: does the structure reveal the mechanism of nature's most proficient enzyme? *Chembiochem*. 2001; 2:113–118. [PubMed: 11828434]
21. Lewis CA Jr, Wolfenden R. Orotic acid decarboxylation in water and nonpolar solvents: a potential role for desolvation in the action of OMP decarboxylase. *Biochemistry*. 2009; 48:8738–8745. [PubMed: 19678695]
22. Crosby J, Lienhard GE. Mechanisms of thiamine-catalyzed reactions. A kinetic analysis of the decarboxylation of pyruvate by 3,4-dimethylthiazolium ion in water and ethanol. *J Am Chem Soc*. 1970; 92:5707–5716. [PubMed: 5458742]
23. Crosby J, Stone R, Lienhard GE. Mechanisms of thiamine-catalyzed reactions. Decarboxylation of 2-(1-carboxy-1-hydroxyethyl)-3,4-dimethylthiazolium chloride. *J Am Chem Soc*. 1970; 92:2891–2900. [PubMed: 5439974]
24. Wood BM, Chan KK, Amyes TL, Richard JP, Gerlt JA. Mechanism of the orotidine 5'-monophosphate decarboxylase-catalyzed reaction: effect of solvent viscosity on kinetic constants. *Biochemistry*. 2009; 48:5510–5517. [PubMed: 19435313]
25. Levine HL, Brody RS, Westheimer FH. Inhibition of orotidine-5'-phosphate decarboxylase by 1-(5'-phospho-beta-D-ribofuranosyl)barbituric acid, 6-azauridine 5'-phosphate, and uridine 5'-phosphate. *Biochemistry*. 1980; 19:4993–4999. [PubMed: 7006681]
26. Datsenko KA, Wanner BL. One-step inactivation of chromosomal genes in Escherichia coli K-12 using PCR products. *Proc Natl Acad Sci U S A*. 2000; 97:6640–6645. [PubMed: 10829079]
27. Otwinowski, Z.; Minor, W. Processing of X-ray diffraction data collected in oscillation mode. In: Carter, CWJ.; Sweet, RM.; Abelson, JN.; Simon, MI., editors. *Methods in Enzymology*. New York: Academic Pres; 1997. p. 307–326.
28. Long F, Vagin AA, Young P, Murshudov GN. BALBES: a molecular-replacement pipeline. *Acta Crystallogr D Biol Crystallogr*. 2008; 64:125–132. [PubMed: 18094476]
29. Emsley P, Cowtan K. Coot: model-building tools for molecular graphics. *Acta Crystallogr D Biol Crystallogr*. 2004; 60:2126–2132. [PubMed: 15572765]
30. Adams PD, Afonine PV, Bunkoczi G, Chen VB, Davis IW, Echols N, Headd JJ, Hung LW, Kapral GJ, Grosse-Kunstleve RW, McCoy AJ, Moriarty NW, Oeffner R, Read RJ, Richardson DC, Richardson JS, Terwilliger TC, Zwart PH. PHENIX: a comprehensive Python-based system for macromolecular structure solution. *Acta Crystallogr D Biol Crystallogr*. 66:213–221. [PubMed: 20124702]
31. Lamzin VS, Wilson KS. Automated refinement for protein crystallography. *Methods Enzymol*. 1997; 277:269–305. [PubMed: 18488314]
32. Wood BM, Amyes TL, Fedorov AA, Fedorov EV, Shabila A, Almo SC, Richard JP, Gerlt JA. Conformational changes in orotidine 5'-monophosphate decarboxylase: "remote" residues that stabilize the active conformation. *Biochemistry*. 2010; 49:3514–3516. [PubMed: 20369850]

33. Barnett SA, Amyes TL, Wood BM, Gerlt JA, Richard JP. Dissecting the total transition state stabilization provided by amino acid side chains at orotidine 5'-monophosphate decarboxylase: a two-part substrate approach. *Biochemistry*. 2008; 47:7785–7787. [PubMed: 18598058]
34. DeLano, WL. The PyMOL Molecular Graphics System. San Carlos, CA: DeLano Scientific LLC; 2002.

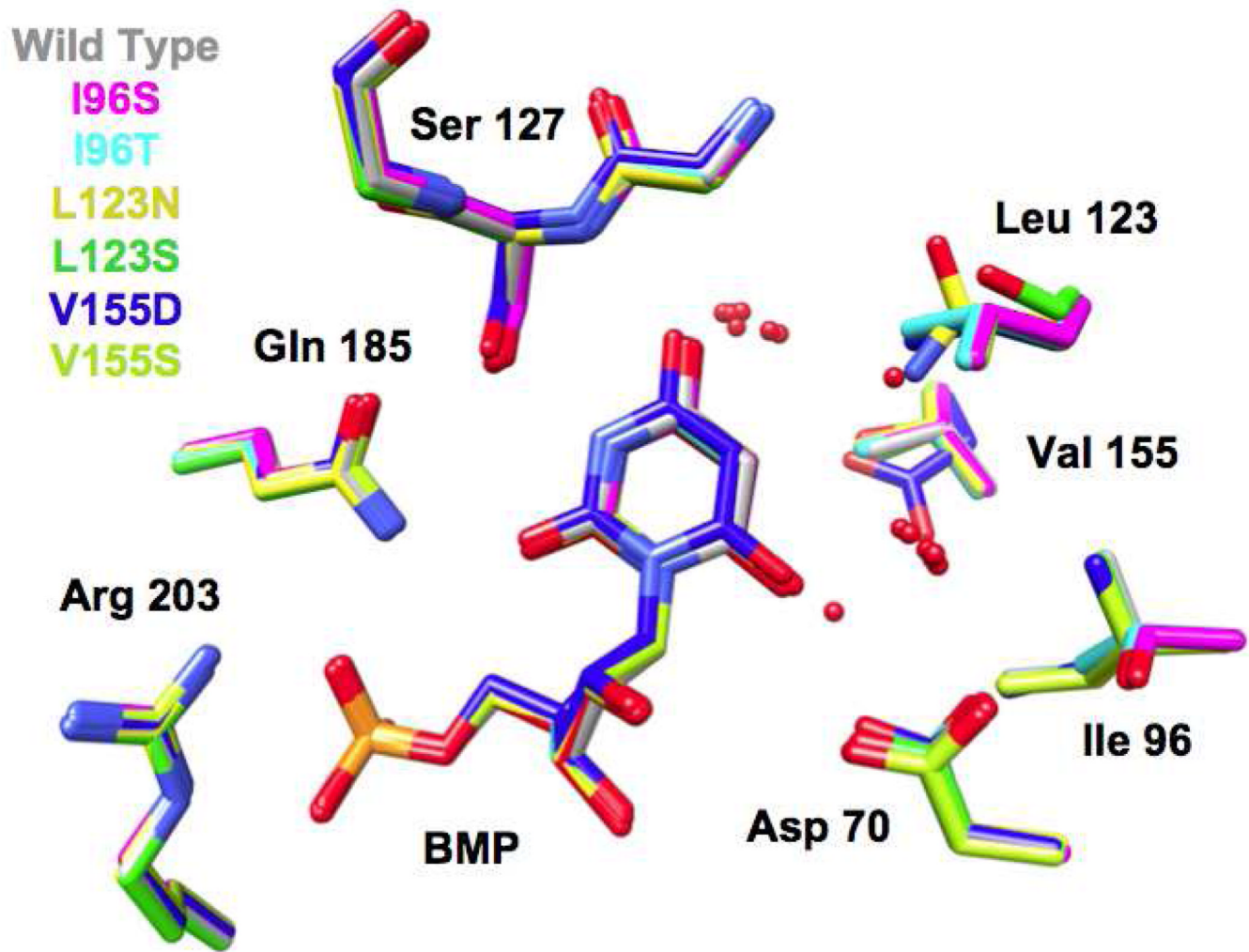
**Figure 1.**

Representative electron density map for the active site of S127P mutant complexed with azaUMP and countered at  $1.5 \sigma$ . The figure was produced with PyMOL (34). The details of the interactions between 6-azaUMP and the active site are described in the text.



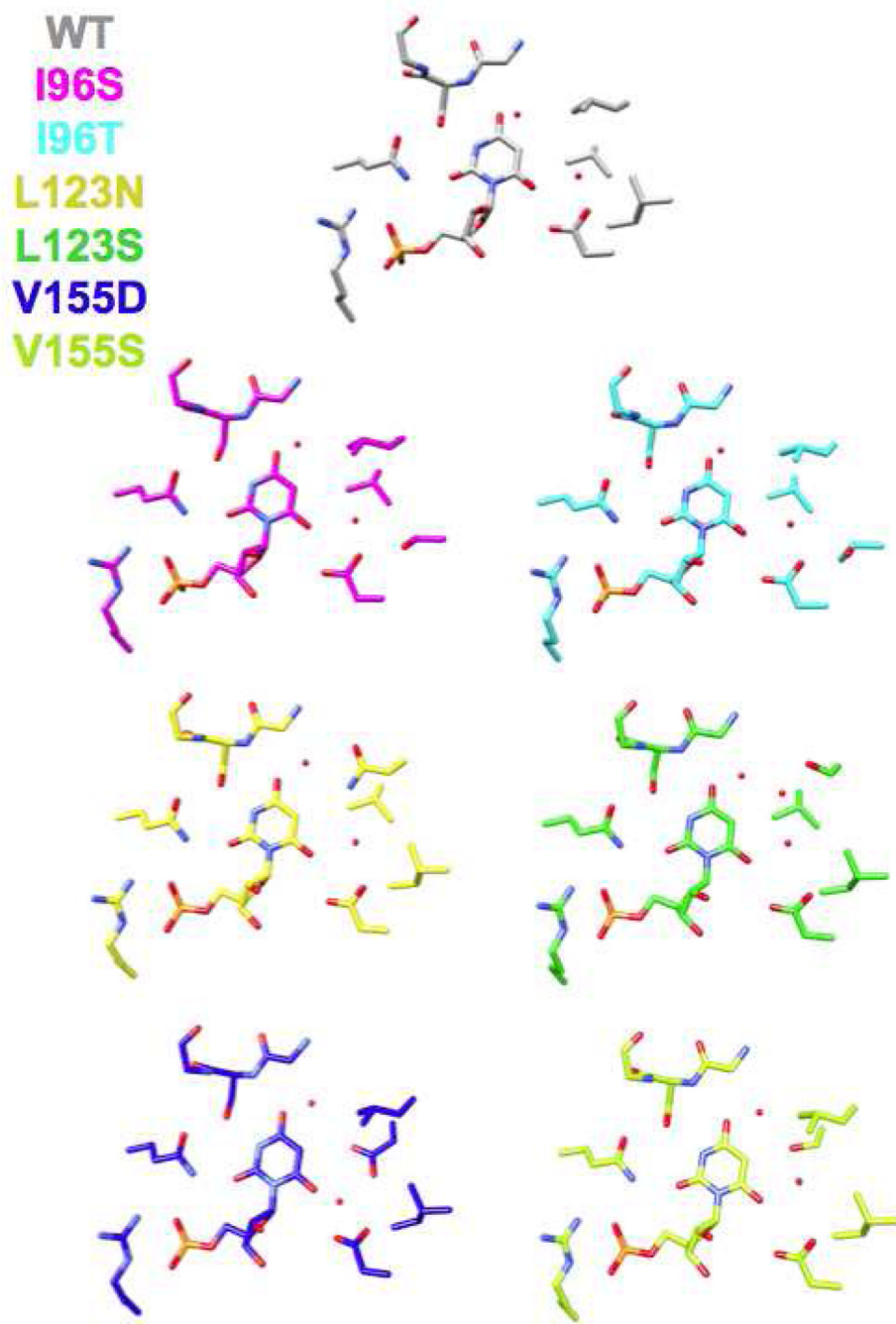
**Figure 2.**

Active site of MtOMPDC liganded with H<sub>2</sub>OMP (4) with the residues that form the hydrophobic pocket represented with space-filling atoms.



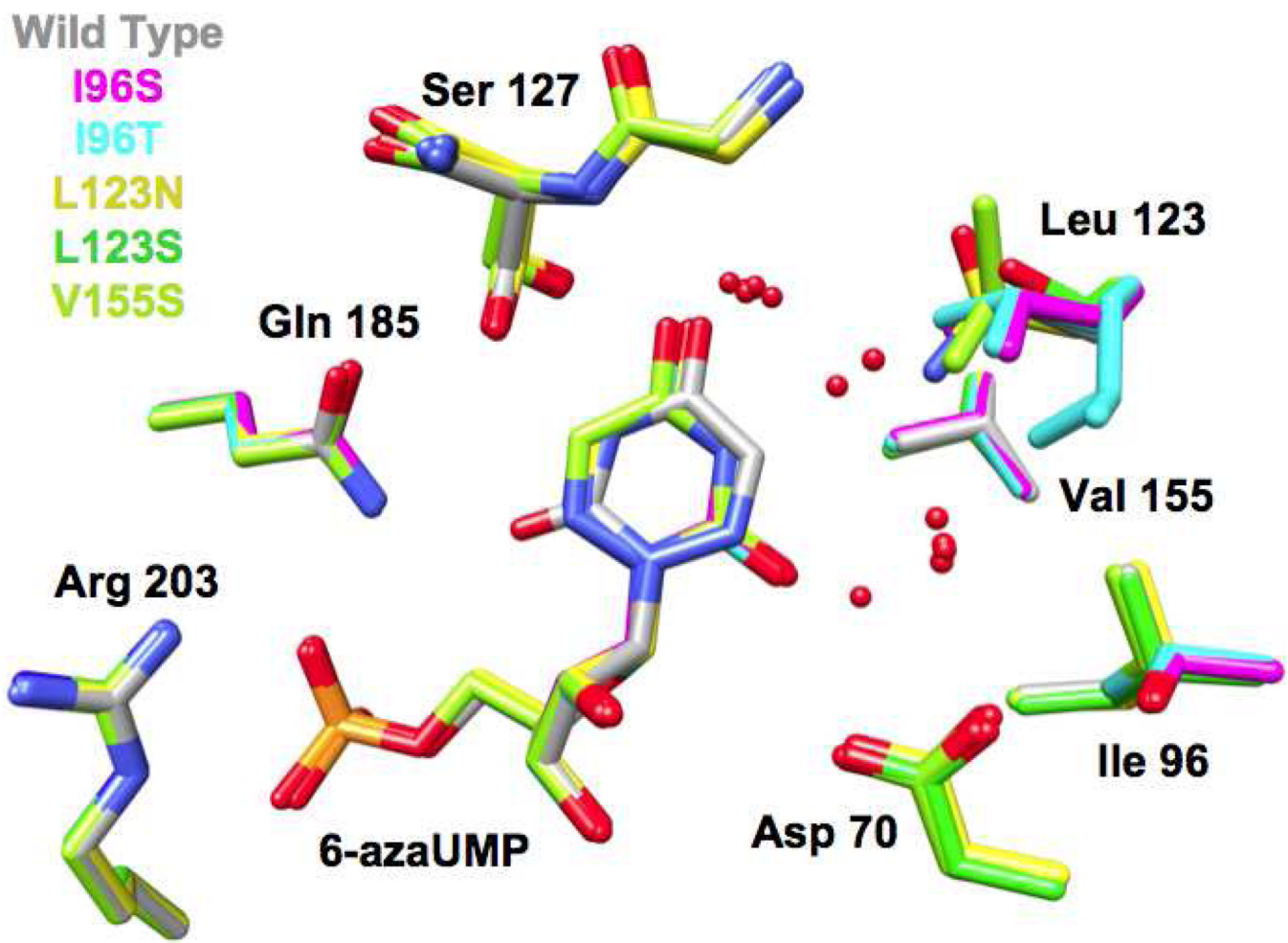
**Figure 3.**

Superposition of the active sites of the hydrophobic pocket mutants liganded with BMP. The red spheres represent water molecules.



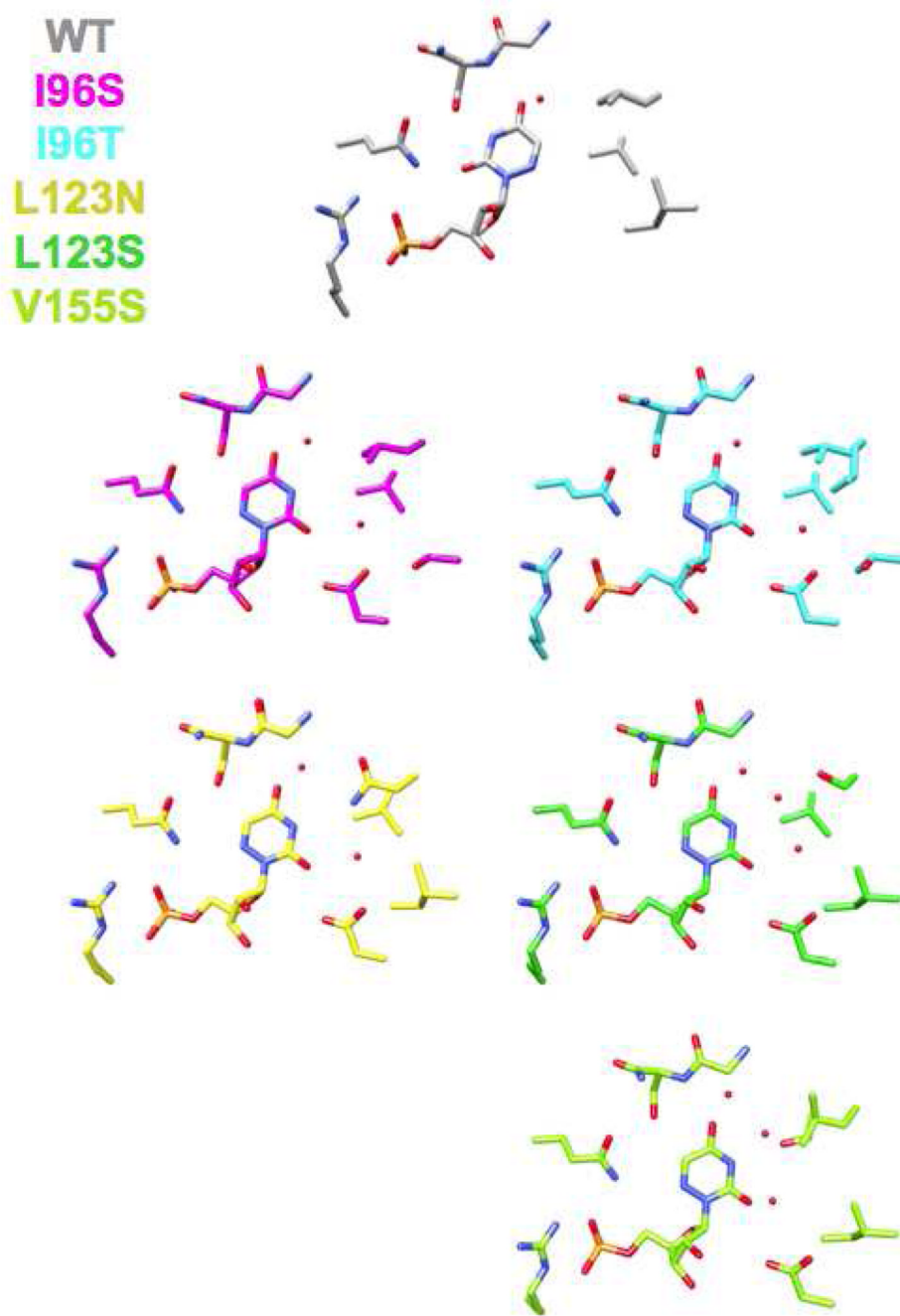
**Figure 4.**

Active sites of the hydrophobic pocket mutants liganded with BMP. The red spheres represent water molecules. All of the active sites contain two spatially conserved water molecules; the active site of L123S contains an additional water molecule hydrogen bonded to the OH group of Ser 123.

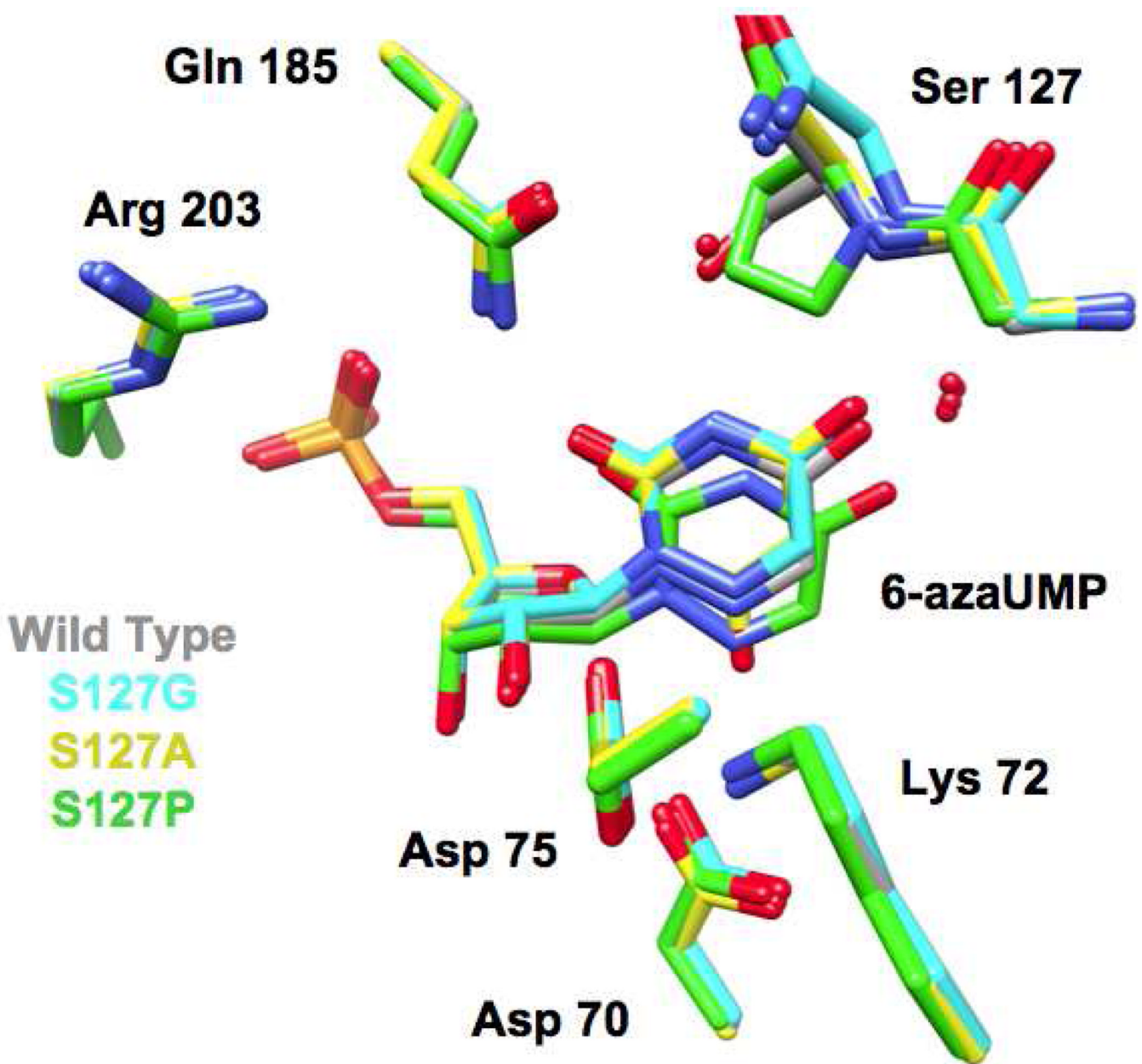


**Figure 5.**

Superposition of the active sites of the hydrophobic pocket mutants liganded with azaUMP.  
The red spheres represent water molecules.

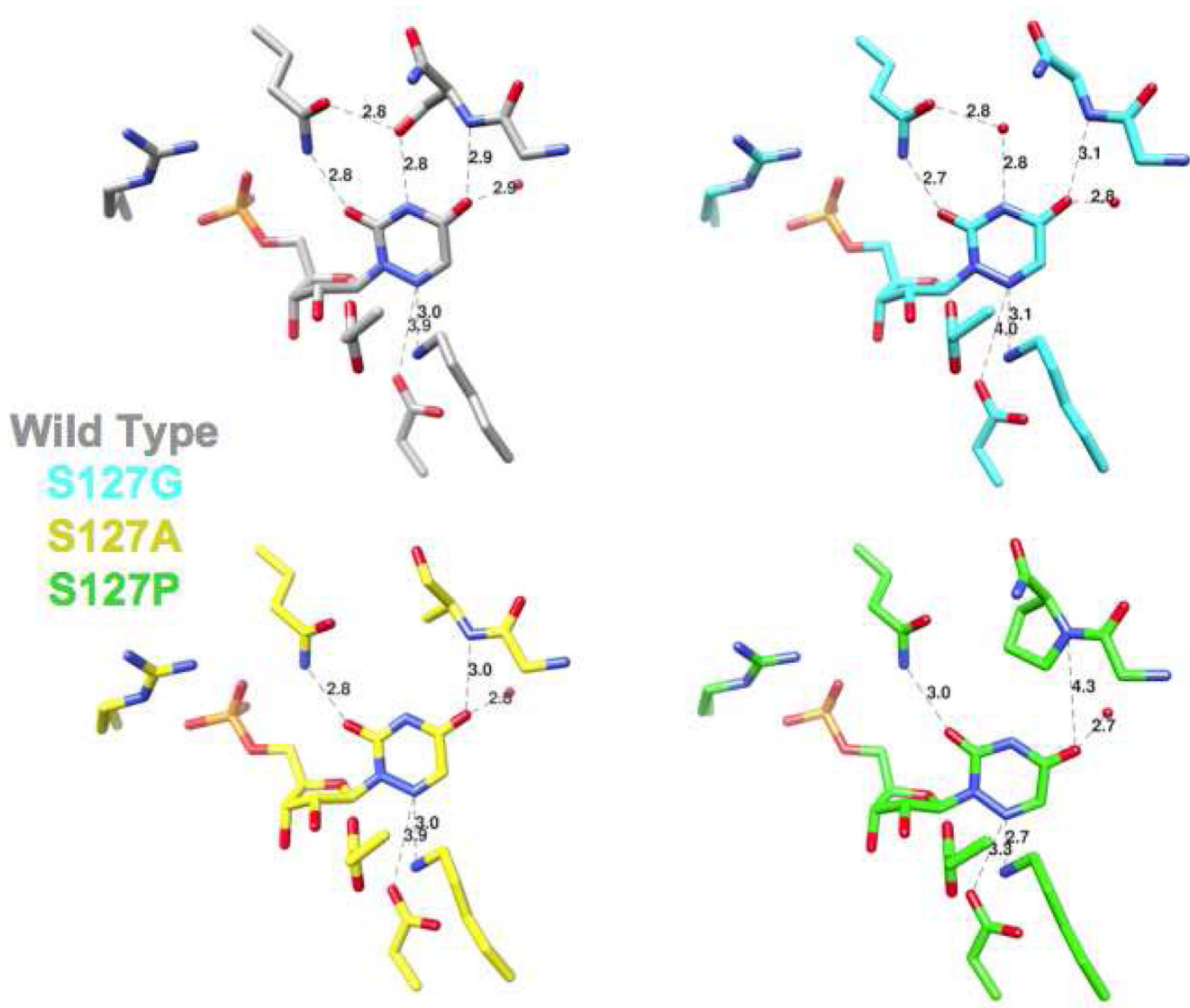
**Figure 6.**

Active sites of the hydrophobic pocket mutants liganded with azaUMP. The red spheres represent water molecules. All of the active sites contain two spatially conserved water molecules; the active sites of L123S and V155S contain an additional water molecule hydrogen bonded to the OH group of Ser 123.

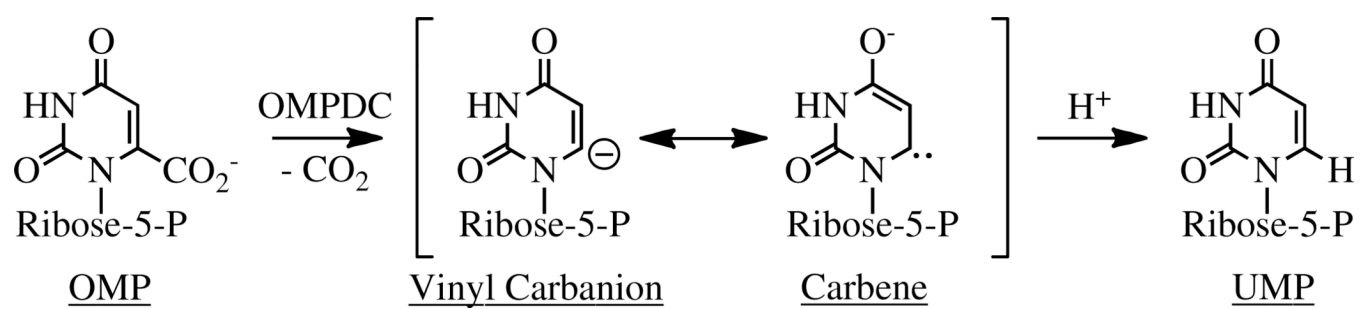


**Figure 7.**

Superposition of the active sites of the mutants of Ser 127 liganded with azaUMP. The red spheres represent water molecules.

**Figure 8.**

Active sites of the mutants of Ser 127 liganded with azaUMP. The red spheres represent water molecules. Distances for important interactions of the ligand with active site residues are shown.



Scheme 1.

Data collection and refinement statistics for azaUMP complexes of MtOMPDC mutants

**Table 1**

	S127G	S127A	S127P	I96S	I96T	L123N	L123S	V155S
<b>Data collection</b>								
Space group	P2 <sub>1</sub>	P2 <sub>1</sub>	P4 <sub>1</sub>	P2 <sub>1</sub>				
No. of molecules	2	2	2	2	2	2	2	2
in asym. unit								
Cell dimensions								
<i>a</i> (Å)	59.78	59.71	56.67	59.79	59.78	59.77	59.71	
<i>b</i> (Å)	63.64	63.60	56.67	64.09	63.95	64.14	64.04	63.83
<i>c</i> (Å)	61.12	61.20	125.95	61.60	61.64	61.61	61.61	61.70
β (°)	115.20	115.19		115.60	115.47	115.55	115.50	115.22
Resolution (Å)	1.45	1.32	1.30	1.30	1.3	1.3	1.3	1.3
No. of unique reflections	68702	96918	91113	99507	97354	101238	97097	92236
<i>R</i> <sub>merge</sub>	0.064	0.059	0.071	0.092	0.083	0.083	0.074	0.069
Completeness (%)	93.4	99.8	93.6	96.3	94.6	98.2	94.3	89.4
<b>Refinement</b>								
Resolution (Å)	25.0-1.45	25.0-1.32	25.0-1.30	25.0-1.3	25.0-1.30	25.0-1.30	25.0-1.3	25.0-1.3
<i>R</i> <sub>cyst</sub>	0.184	0.196	0.234	0.223	0.161	0.161	0.160	0.175
<i>R</i> <sub>free</sub>	0.216	0.218	0.258	0.247	0.183	0.175	0.169	0.193
No. atoms								
Protein	3296	3396	3294	3378	3404	3464	3410	3402
Waters	522	405	308	348	463	482	419	398
Bound ligand	6azaUMP							
Ligand atoms	42	42	42	42	42	42	42	42
R.m.s deviations								
Bond lengths (Å)	0.004	0.006	0.005	0.006	0.006	0.006	0.006	0.006
Bond angles (°)	1.2	1.0	1.2	1.1	1.1	1.1	1.1	1.1

PDB entry	S127G	S127A	S127P	I96S	I96T	L123N	L123S	V155S
	3LLD	3SY5	3LLF	3PRU	3RPV	3PBW	3PY	3PCO

Data collection and refinement statistics for BMP complexes MtOMPDC mutants

**Table 2**

	<b>S127A</b>	<b>I96S</b>	<b>I96T</b>	<b>L123N</b>	<b>L123S</b>	<b>V155D</b>	<b>V155S</b>
<b>Data collection</b>							
Space group	P2 <sub>1</sub>						
No. of molecules in asym. unit	2	2	2	2	2	2	2
<b>Cell dimensions</b>							
<i>a</i> (Å)	59.89	59.93	59.97	59.92	59.85	59.74	59.71
<i>b</i> (Å)	64.16	64.34	63.84	63.98	63.93	64.33	64.28
<i>c</i> (Å)	61.57	61.58	61.58	61.75	61.74	61.55	61.33
β (°)	115.60	115.86	115.54	115.56	115.57	115.53	115.54
Resolution (Å)	1.32	1.53	1.42	1.42	1.31	1.42	1.32
No. of unique reflections	98290	63155	76659	78628	95704	77594	97409
<i>R</i> <sub>merge</sub>	0.071	0.087	0.063	0.079	0.089	0.058	0.091
Completeness (%)	99.8	99.4	97.7	99.3	95.5	97.9	99.26
<b>Refinement</b>							
Resolution (Å)	25.0-1.32	25.0-1.53	25.0-1.42	25.0-1.42	25.0-1.31	25.0-1.42	25.1-1.32
<i>R</i> <sub>cryst</sub>	0.172	0.161	0.164	0.180	0.165	0.174	0.164
<i>R</i> <sub>free</sub>	0.193	0.186	0.185	0.205	0.177	0.202	0.177
No. atoms							
Protein	3422	3388	3364	3388	3414	3404	3386
Waters	424	358	393	432	468	387	465
Bound ligand	BMP						
Ligand atoms	44	44	44	44	44	44	44
<b>R.m.s deviations</b>							
Bond lengths (Å)	0.006	0.006	0.006	0.006	0.006	0.006	0.006
Bond angles (°)	1.05	1.08	1.09	1.10	1.11	1.07	1.11

PDB entry	S127A	I96S	I96T	L123N	L123S	V155D	V155S
	3S1Z	3NQD	3NQC	3NQE	3NQF	3NQG	3NQM

**Table 3**  
Kinetics of Hydrophobic Pocket Mutants

OMPDC	$k_{cat}$ (s <sup>-1</sup> )	K <sub>M</sub> (μM)	$k_{cat}/K_M$ (M <sup>-1</sup> s <sup>-1</sup> )	$k_{ex}$ (s <sup>-1</sup> )
WT	4.0 ± 0.2	1.6 ± 0.1	2.0 × 10 <sup>6</sup>	0.015 ± 0.004
I96T	0.69 ± 0.05	2.3 ± 0.06	3.0 × 10 <sup>5</sup>	0.0047 ± 0.0004
I96S	0.011 ± 0.002	1.0 ± 0.04	1.0 × 10 <sup>4</sup>	0.006 ± 0.001
L123N	0.64 ± 0.01	3.5 ± 0.2	1.9 × 10 <sup>5</sup>	0.0007 ± 0.0001
L123S	0.36 ± 0.04	3.0 ± 0.5	1.2 × 10 <sup>5</sup>	0.00039 ± 0.00001
V155S	0.011 ± 0.003	4.7 ± 0.1	2.2 × 10 <sup>4</sup>	0.006 ± 0.003
V155D	5 ± 2 × 10 <sup>-4</sup>	4.6 ± 0.5	4.6 × 10 <sup>2</sup>	0.057 ± 0.002
D70N	0.024 ± 0.05	6.0 ± 0.3	4.0 × 10 <sup>3</sup>	0.005 ± 0.002
D70N/I96S	6.0 (± 1.0) × 10 <sup>-5</sup> (5) <sup>a</sup>	-	-	0.002 ± 0.0003 (0.13) <sup>d</sup> (22) <sup>a</sup>
D70N/L123S	9.3 (± 0.1) × 10 <sup>-4</sup> (0.1) <sup>b</sup>	-	-	0.00001 ± 0.000007 (1500) <sup>e</sup> (1.7) <sup>b</sup>
D70N/V155S	1.8 ± (0.4) × 10 <sup>-4</sup> (1.5) <sup>c</sup>	-	-	0.0019 ± 0.0006 (0.13) <sup>f</sup> (44) <sup>c</sup>

<sup>a</sup>(D70N/I96S) / (D70N)(I96S)<sup>b</sup>(D70N/L123S) / (D70N)(L123S)<sup>c</sup>(D70N/V155S) / (D70N)(V155S)<sup>d</sup>(D70N/I96S) / (D70N)<sup>e</sup>(D70N/L123S) / (D70N)<sup>f</sup>(D70N/V155S) / (D70N)

**Table 4**

## Kinetics of Ser 127 Mutants

OMPDC	$k_{cat}$ (s <sup>-1</sup> )	K <sub>M</sub> (μM)	$k_{cat}/K_M$ (M <sup>-1</sup> s <sup>-1</sup> )
WT	4.6 ± 0.4	2.1 ± 0.1	2.2 (± 0.2) × 10 <sup>6</sup>
S127A	0.035 ± 0.002	96 ± 5	3.6 (± 0.3) × 10 <sup>2</sup>
S127G	0.26 ± 0.007	59 ± 5	4.3 (± 0.3) × 10 <sup>3</sup>
S127P	-	-	0.88 ± 0.16 <sup>a</sup>

<sup>a</sup>Velocity is directly proportional to substrate concentration.